Geophys. J. Int. (2002) **149,** 118–133

Non-linear waveform inversion for surface waves with a neighbourhood algorithm—application to multimode dispersion measurements

K. Yoshizawa and B. L. N. Kennett

Research School of Earth Sciences, The Australian National University, Canberra ACT 0200, *Australia. E-mail: kazu@rses.anu.edu.au*

Accepted 2001 October 8. Received 2001 October 8; in original form 2001 May 30

SUMMARY

A new technique for multimode dispersion measurement has been developed by employing fully non-linear waveform inversion for a path-specific 1-D profile using a neighbourhood algorithm (NA). One-dimensional models derived from waveform inversion are quite sensitive to the model parametrization and the reference model used to start the inversion. With different approaches to the parametrization of the shear wave speed profile, we can find models with significant differences in velocity variation with depth, which provide similar levels of fit to the observed waveforms. Although the models differ, the calculated phase dispersion for the first few modes of the surface waves are very close indeed. We therefore regard the 1-D models derived from the multimode waveform inversion as an implicit description of the path-specific dispersion for each of the modes. The inversion procedure using NA samples a substantial number of models and we select the 1-D wave speed model that achieves minimum misfit. Phase speeds for each mode branch are then calculated from the model parameters with the minimum misfit. Because we use the 1-D models as a summary of the average multimode dispersion along the path, we do not need to make assumptions concerning the nature of anisotropy. We can employ simple isotropic models and the method can be applied to both Rayleigh and Love waves independently. The new method is applied to sets of paths in the Australian region and provides stable measurements of multimode dispersion from a single seismogram. The multimode phase speeds measured using the NA inversion can be used to retrieve phase velocity maps as a function of frequency for higher-mode branches as well as the fundamental mode, which will be crucial constraints on 3-D Earth models.

Key words: multimode dispersion, neighbourhood algorithm, surface wave, tomography, waveform inversion.

1 INTRODUCTION

Current methods of surface wave tomography have been based on multistage processes. The first step in such methods is to invert multimode waveforms for a path-averaged 1-D model for which calculated waveforms match suitably filtered observations (e.g. Cara & Lévêque 1987; Nolet 1990) or to measure phase or group dispersion directly (e.g. Ekström *et al.* 1997, Ritzwoller & Levshin 1998).

Waveform inversion for 1-D models is common in regional studies and should have a good resolution in depth since constraints from higher-mode branches can be included in the inversion. However, the resultant path-specific 1-D models are quite sensitive to the model parametrization and to the reference model used to start the non-linear inversion, resulting in significant non-uniqueness of 1-D models, which achieve an adequate fit to the observations. Direct dispersion measurements have been utilized in most global studies and allow the extraction of stable results from observations without any interference from the style of model parametrization. However, the depth resolution can be rather limited because direct dispersion measurements can only be applied readily to fundamental modes. It is also possible to measure phase dispersion using waveform inversion with a parametrization for phase speed perturbation (e.g. Trampert & Woodhouse 1995), although such techniques still have difficulties in the use of higher modes.

In order to exploit the advantages of the different methods, whilst avoiding their deficiencies, multimode dispersion measurement would be desirable. Multimode information is essential for enhancing the depth resolution of surface-wave tomography models. Techniques for measuring higher-mode phase speed have mainly been based on the concept of 'mode separation'. One of the traditional ways to isolate overlapped higher modes is to apply a frequency–wavenumber filter to stacked waveforms observed in a seismograph network (e.g. Nolet 1975; Cara 1978).

Measuring multimode dispersion from a single seismogram is not a straightforward issue. Stutzmann & Montagner (1993) used a set of seismograms recorded at a single station with several sources at different depths in a small epicentral area to obtain reliable multimode dispersion measurements. This requirement of similar source–receiver pairs reduces the number of available paths dramatically. van Heijst & Woodhouse (1997) developed a 'mode branch stripping' technique by using mode branch cross-correlation functions. In this method, phase speeds for a mode branch are measured by fitting the cross-correlation function for the mode, then the fit to the mode branch seismogram is removed from the observed seismogram and the process is repeated for the next mode branch. This technique is quite effective especially in the case of longer paths for which higher-mode branches do not overlap each other in a seismogram (van Heijst & Woodhouse 1999). However, it cannot readily be applied to regional studies for which the most paths are shorter than 30° and individual higher-mode contributions can hardly be distinguished in a seismogram.

In this paper we propose a new technique of multimode dispersion measurement using non-linear waveform inversion for surface waves, especially for regional surface waves. The process of waveform inversion depends on knowledge of the source mechanism and is quite sensitive to the starting model with consequent ambiguities in the model. Therefore, there are advantages in adopting a direct non-linear approach (without linearization) which does not require the evaluation of derivatives with respect to the model parameters. We adopt the neighbourhood algorithm of Sambridge (1999a) (hereafter referred to as NA) which enables us to explore a model parameter space so as to best fit the observations.

We take a different viewpoint from the current style of waveform inversion, and do not consider the path-specific 1-D models as a direct representation of the Earth model, but instead we interpret them as providing implicit information on multimode dispersion for the source–receiver path. If the perturbations from the reference model are weak it may be justified to interpret the 1-D models themselves as an average along the path, but the waveform inversion does not depend on this assumption (Kennett & Yoshizawa 2001). The 1-D models derived from waveform inversions depend significantly on the parametrization and the reference model. Even though models differ, synthetic waveforms for the models match well to observations, suggesting that the multimode dispersion is well represented through the process of waveform fitting. The multimode phase speeds derived for the various paths can be used to reconstruct multimode dispersion maps that will provide crucial information for reconstructing 3-D shear wave speed structure.

2 METHOD OF NON-LINEAR WAVEFORM INVERSION

The process of waveform inversion is highly non-linear and the results depend on knowledge of the source mechanism, the parametrization of the model and the choice of a reference model. Thus a fully non-linear approach, which does not require any calculations of derivatives with respect to model parameters, is desirable for the purpose of waveform matching. We adopt the neighbourhood algorithm of Sambridge (1999a) as a global optimizer that explores the model parameter space to find the models with the best fit to the data. The procedure of non-linear waveform fitting using the NA can be summarized as follows:

(1) generate a path-specific 1-D shear wave speed model using NA;

(2) compute a synthetic seismogram for the 1-D model;

(3) calculate the misfit between synthetic and observed waveforms;

(4) repeat (1)–(3) until N models are calculated;

(5) compute phase dispersion from the best-fitting 1-D model;

(6) estimate reliability of the dispersion measurement.

2.1 Neighbourhood algorithm

The NA is based on simple principles and can be used a as global optimizer. The details of the NA are fully described in Sambridge (1999a), and here we only explain the method briefly. The feature of the NA is that model parameter space is divided into Voronoi (nearest-neighbour) cells defined by a suitable distance norm (usually L_2) and a search is made over models within cells with the aim of finding a smaller misfit. At each stage (iteration) Voronoi cells are defined uniquely by the previous samples. These irregular polyhedra guide subsequent samples and the algorithm is able to concentrate sampling in favourable regions of parameter space. Only two tunable parameters are necessary, and no derivatives with respect to the model parameters are required. The neighbourhood algorithm takes the following form:

(a) generate a set of n_s models uniformly in parameter space;

(b) calculate misfit for the latest n_s models and choose n_r models with the smallest misfits of all the generated models;

(c) n_s new models are generated from a random walk in the Voronoi cell of each of n_r chosen models;

(d) repeat (b) and (c).

As mentioned in Sambridge (1999a), the choice of NA parameters n_s and n_r is arbitrary and there is as yet no quantitative ways to determine the optimal values of these parameters. We have performed a number of trials with various combinations of n_s and n_r, and we decided to use the NA method with $n_s = 10$ and $n_r = 5$. 300 iterations are performed so that 3000 models are generated for each inversion.

2.2 Waveform inversion for 1-D models

The surface waveforms for a reference model are approximated asymptotically as a sum of several mode branches as

$$u^0(\Delta, \omega) = \sum_{j=0}^{J} R_j^0(\omega) \exp\left[i k_j^0(\omega)\Delta\right] S_j^0(\omega), \tag{1}$$

where R_j^0 represents the receiver term, geometrical spreading and attenuation and S_j^0 is the source excitation for the j th mode branch, k_j^0 is a path-averaged wavenumber along a great-circle, Δ is the epicentral distance and ω is the angular frequency.

In the presence of slight lateral heterogeneity, the waveforms can be described approximately by a perturbation of the wavenumber,

$$u(\Delta, \omega) = \sum_{j=0}^{J} R_j(\omega) \exp\left\{i\left[k_j^0(\omega) + \delta k_j(\omega)\right]\Delta\right\} S_j(\omega), \tag{2}$$

where R_j and S_j are the receiver and source terms for the actual Earth and $\delta k_j(\omega)$ is the wavenumber perturbation induced by the variations along the path. From the asymptotic results of Woodhouse (1974) for a smoothly varying model, δk_j is built from the path-average of the local wavenumber perturbations. The final form is equivalent to a perturbation of a 1-D model. Throughout this study, R_j and R_j^0 as well as S_j and S_j^0 are assumed to be identical.

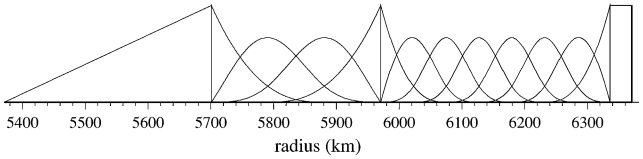

Figure 1. Representation of a model-parameter set using *B*-spline functions. Three discontinuities at Moho, 400 and 670 km are included in the model parametrization and, within each layer, the shear wave speed perturbation varies smoothly as a sum of the *B*-splines.

When we perform fully non-linear inversions for surface waveforms, it would be desirable to undertake a full recalculation of seismograms by computing normal or surface-wave modes for each new model. However, this places very heavy computational demands and is not a practical way to perform waveform inversions with a global optimization technique such as NA, because such global search methods need to generate a large number of models to find some acceptable models. We have therefore employed perturbation analysis from a reference model, which does not require any recalculation of the normal modes, to update the seismograms for new models derived from the NA.

Assuming that the perturbation of wavenumber depends mainly on shear wave speed and the perturbation of wave speed is not so

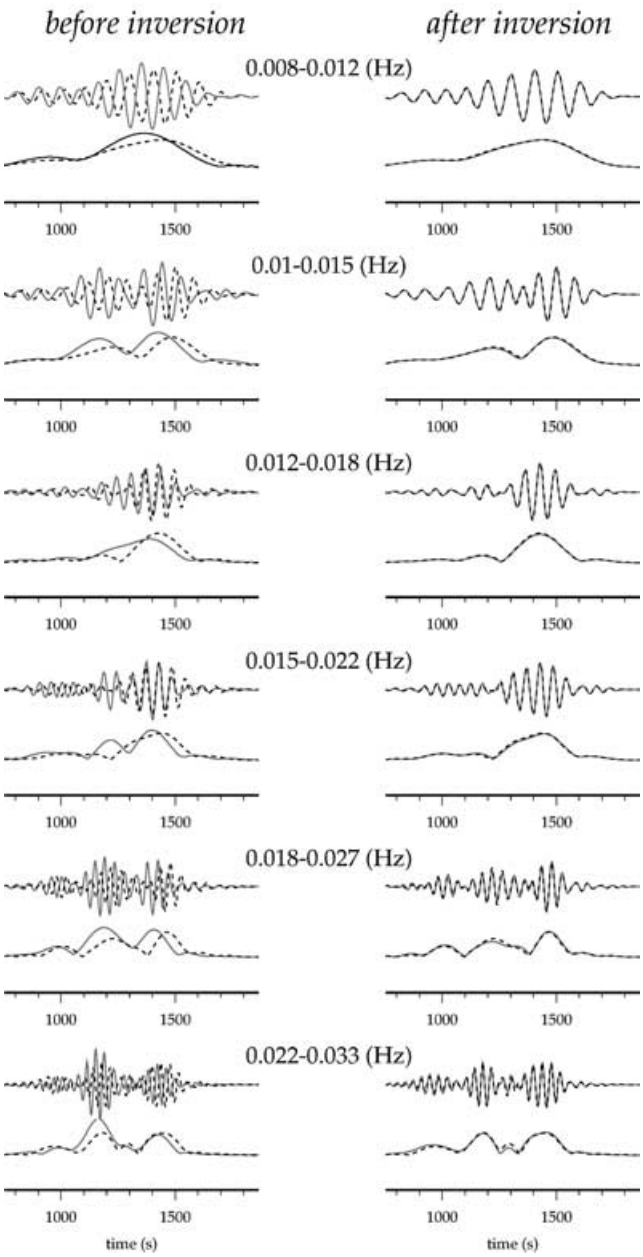

Figure 2. Examples of waveform and envelope fits for six frequency ranges before (left-hand column) and after (right-hand column) NA inversion.

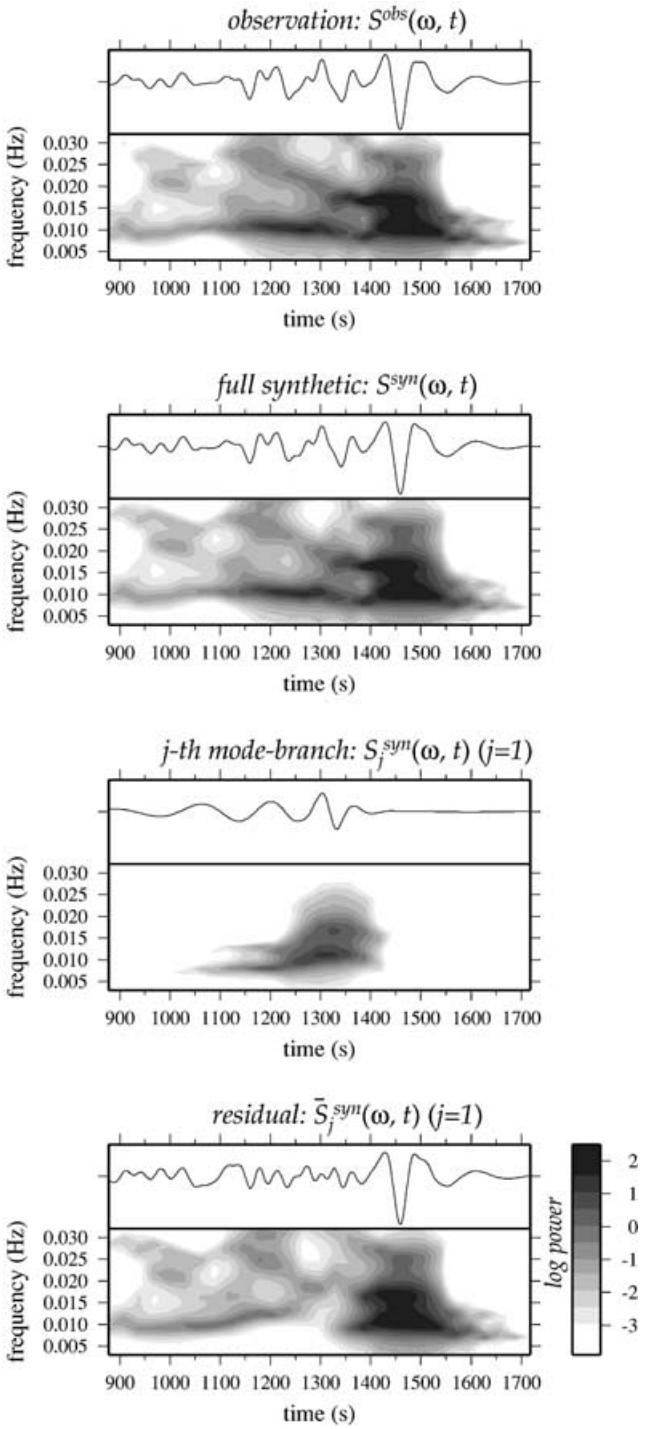

Figure 3. Examples of observed, full synthetic, first higher-mode synthetic and residual seismograms for the best-fitting model derived from a synthetic test (test I) in Fig. 5. Spectrograms are shown below the corresponding seismograms, and are used in the reliability analysis in Fig. 4.

large, δk_j can be represented as the result of the path-averaged shear wave speed perturbation $\delta\beta(z)$ as a function of depth z,

$$\delta k_j(\omega) = \int_0^a K_\beta^j(\omega, z)\, \delta\beta(z)\, dz, \tag{3}$$

where a is the radius of the Earth, $K_\beta^j(\omega, z)$ is the Frechét derivative or sensitivity kernel of the shear wave speed for the jth mode (Takeuchi & Saito 1972; Dahlen & Tromp 1998) which are calculated for a reference model. In this study, the P-wave speed, density and Q of a reference Earth model are fixed and no perturbation of these variables is considered, since they have little influence on the phase speed perturbation for surface waves in the intermediate period range (50–130 s) that is of interest in our study. $\delta\beta$ can be expanded into a set of B-spline functions as

$$\delta\beta = \sum_{i=M} b_i B_i(z), \tag{4}$$

where M is the total number of parameters, $B_i(z)$ is the ith B-spline function and the corresponding coefficient b_i is a model parameter, which should be obtained from the NA sampling.

An example of the parametrization of the crust and upper mantle using the B-splines is shown in Fig. 1. We divide the shear wave speed model into four layers with three boundaries at the depth of Moho, 400 and 670 km, where $B_i(z)$ is discontinuous. The number of parameters in each layer is adjustable for each inversion (M_1, 0–Moho; M_2, Moho–400 km; M_3, 400–670 km; and M_4, below 670 km, the total number of parameters $M = \sum_{i=1}^{4} M_i$).

One of the important factors in waveform inversion based on the perturbation theory is to choose an appropriate reference model. In

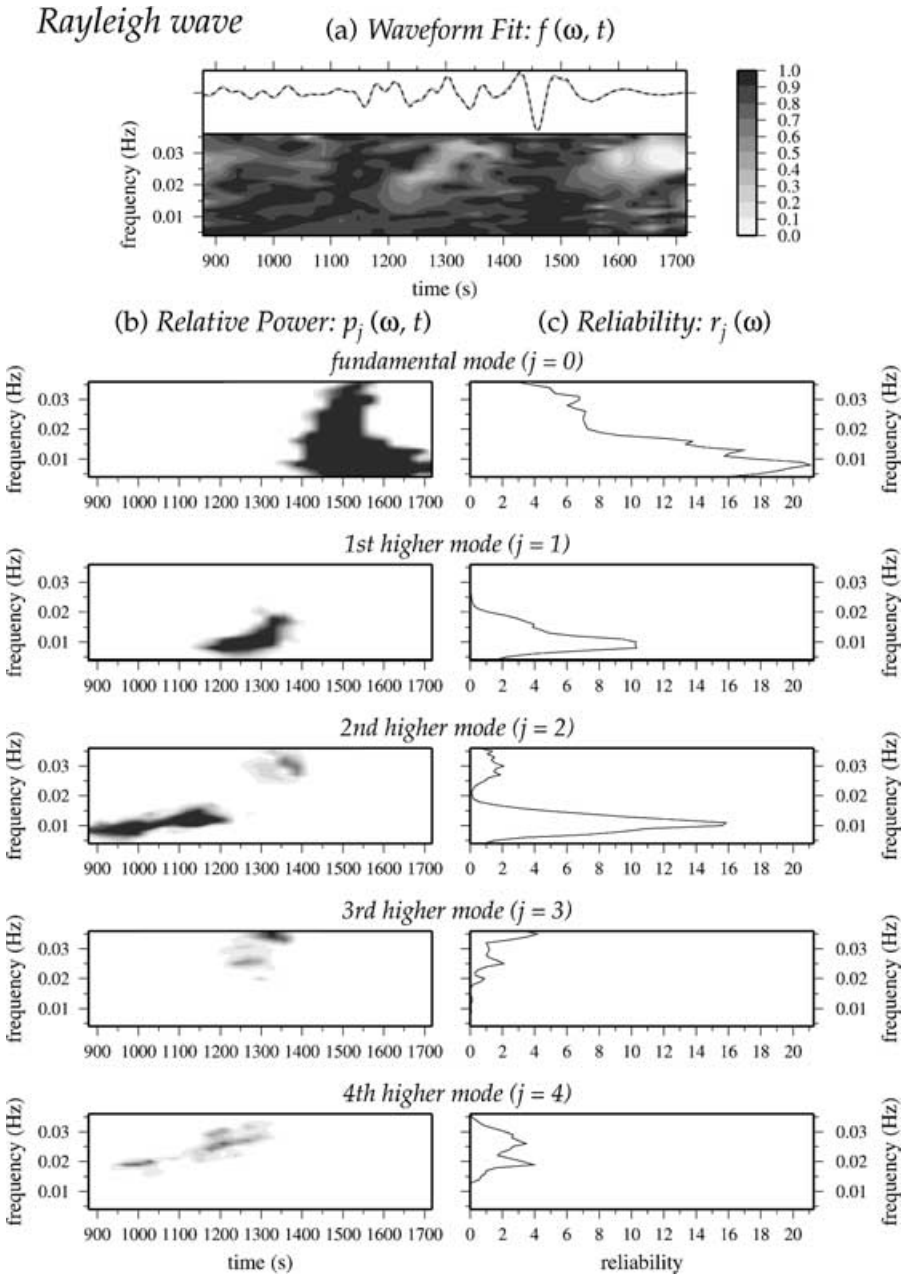

Figure 4. Diagrams of the waveform fit $\mathbf{f}(\omega, t)$, the relative power in the jth mode $\mathbf{p}_j(\omega, t)$ and the reliability parameter $r_j(\omega)$ for the first five mode branches calculated from the results of test I in Fig. 5.

this study, we mainly use PREM (Dziewonski & Anderson 1981) or PREMC, for which the upper-mantle structure is modified to provide a better representation of continental regions. The discontinuity at 220 km depth in the PREM model is modified so that shear wave speeds around 220 km are smoothly varying. The crustal structures are corrected using the 3SMAC model (Nataf & Ricard 1996). For regional surface-wave paths passing through regions with strong velocity anomalies, such spherical Earth models cannot be the best choice for the waveform inversion. Since we treat each observation independently, we do not need to use a single or a particular reference model for different paths. We have devised a procedure for obtaining a path-specific reference model by assessing the phase-speed perturbation of the fundamental-mode surface waves using a spherical Earth model. The details of the technique are described in Appendix A. The data adaptive selection of a reference model has been adopted in the actual waveform inversion in Section 5.

2.3 Fitting multiband-pass filtered waveforms and envelopes

Unlike traditional linearized inversion, NA does not require any derivatives with respect to model parameters. Therefore, any type

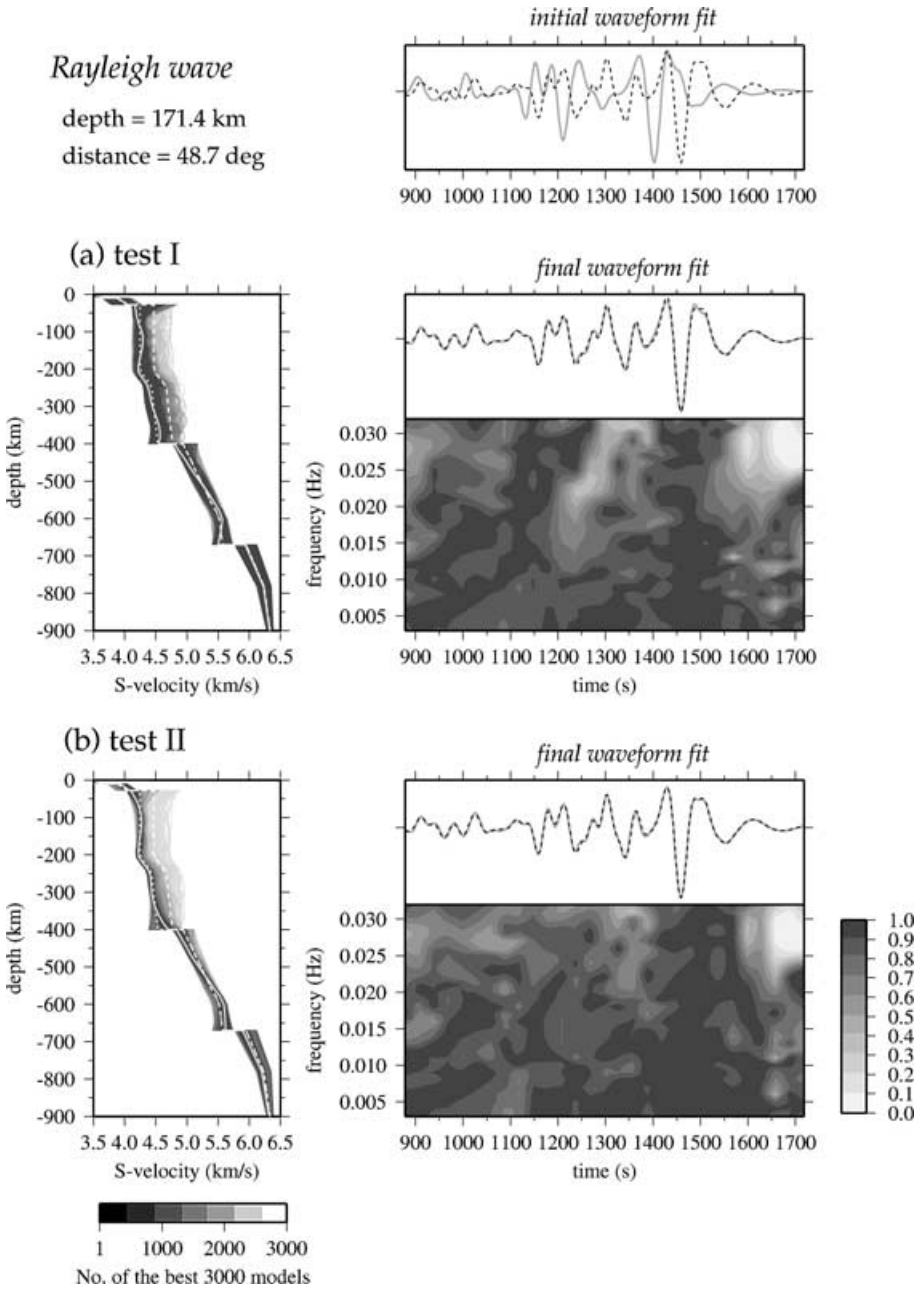

Figure 5. Results of NA inversion for a synthesized Rayleigh wave. Density plots of the 3000 shear wave speed models derived from synthetic tests with a −5 per cent perturbed model are shown in left column. The models are ranked in order of increasing misfit. The best-fitting model is drawn in a solid white line, the reference model in a dashed white line and the true model in a dotted white line. The number of parameters used in test I is 16 ($M_1 = M_4 = 1$, $M_2 = 10$ and $M_3 = 4$) and in test II is 12 ($M_2 = 6$ and others are the same as in test I). The initial and final fits for the waveforms are displayed in the right-hand column together with diagrams of the fit in the F-T domain. Synthetic waveforms for the true model are drawn in a dotted line and for the best-fitting models in a solid grey line.

of misfit function can be used to measure the difference between observed and synthetic seismograms. In order to obtain the best-fitting waveform for all frequency ranges of interest, several bandpass filters are applied to seismograms and a set of filtered seismograms with different frequency ranges ($F_i u(t), i = 1, \ldots, n_\mathrm{f}$, where F_i is the ith filter and n_f is the number of frequency ranges) is generated for both observed and synthetic seismograms (Fig. 2). Before applying the bandpass filters, a time window is extracted with appropriate group velocity ranges so that several higher modes as well as the fundamental mode are included in a time-series.

When the difference between a reference model and a true model is significant, 'phase-cycle skip' can be caused by $2n\pi$ ambiguities in phase and this obscures the fit to the waveforms. This problem is common in direct phase measurement methods, and the problem can generally be cured by organizing the measurements of the phase of waveforms from lower to higher frequency. This approach assumes that the phases of the seismograms are smoothly varying with frequency and that the phase perturbation at lower frequencies should not be larger than π. Here, all bandpass-filtered seismograms are inverted at the same time, so that the traditional approach cannot be used. Instead, we introduce the envelopes, $E\{F_i u(t)\}$, for each filtered seismogram, and match these as well. This gives a significant improvement in waveform fitting when higher modes are included in a time window and several peaks exist in an envelope (Fig. 2). The introduction of envelope fitting can be regarded as fitting the group slowness, as well as the phase slowness which dictates the details of waveforms themselves.

The misfit functions are defined from the filtered seismograms $F_i u(t)$ and their envelopes $E\{F_i u(t)\}$ as follows:

$$\Phi = \sum_{i=1}^{n_\mathrm{f}} \int \left[\left| F_i u^{\mathrm{obs}}(t) - F_i u^{\mathrm{syn}}(t) \right|^p + w_i \left| E\left\{F_i u^{\mathrm{obs}}(t)\right\} - E\left\{F_i u^{\mathrm{syn}}(t)\right\} \right|^p \right] dt, \quad (5)$$

where w_i is the weighting factor for the ith filtered envelope. p represents the order of the misfit norm. We adopt an L_3 norm ($p = 3$) to measure the difference between observed and synthetic waveforms since this is very sensitive to discrepancies in the waveforms or envelopes. We have employed five to seven bandpass filters with overlapping frequency ranges. The envelope fit is helpful for stabilizing the waveform fitting by avoiding phase-cycle skips, especially when we apply an appropriate set of weighting factors $\{w_i\}$. Too large or too small $\{w_i\}$ tends to counteract the waveform fit. After several trials, we decided to use $w_i = 1.5$ for all the waveform inversions in this study.

Since the ranges of frequency and the relative amplitude of the mode branches contained in a seismogram depend strongly on the excitation at the source, weighting factors can be applied to both the filtered seismograms and envelopes to enhance or to reduce the contribution of some particular frequency ranges in the inversion.

3 MULTIMODE DISPERSION MEASUREMENT

3.1 Phase speed estimation from 1-D shear wave speed models

The 1-D models derived from the non-linear waveform inversion are quite non-unique and several different models can provide a reasonably good waveform fit. In this study, we do not interpret such 1-D models obtained from the inversion as an actual Earth model, but we use them as a representation of the multimode dispersion of surface waves.

The path-averaged phase speed perturbation for the jth mode, $\delta c_j(\omega)$, can be calculated simply from the wavenumber perturbation as follows:

$$\frac{\delta c_j(\omega)}{c_j^0(\omega)} = -\frac{\delta k_j(\omega)}{k_j^0(\omega)}, \quad (6)$$

where $c_j^0(\omega)$ is the phase speed for a reference model.

Using the ensemble of models sampled by NA, we can estimate approximate errors in the dispersion measurement. Resampling of models using NA would be an appropriate way to estimate errors from the ensemble of models (Sambridge 1999b), but the resampling process is computationally demanding and as for any Bayesian approach we would also need to characterize the statistics of all the noise processes involved (which is not a trivial task). In this study, we roughly estimate errors of the dispersion measurements from the standard deviations of dispersion curves for the best 1000 models without resampling of the models. Averages of the best 1000 models

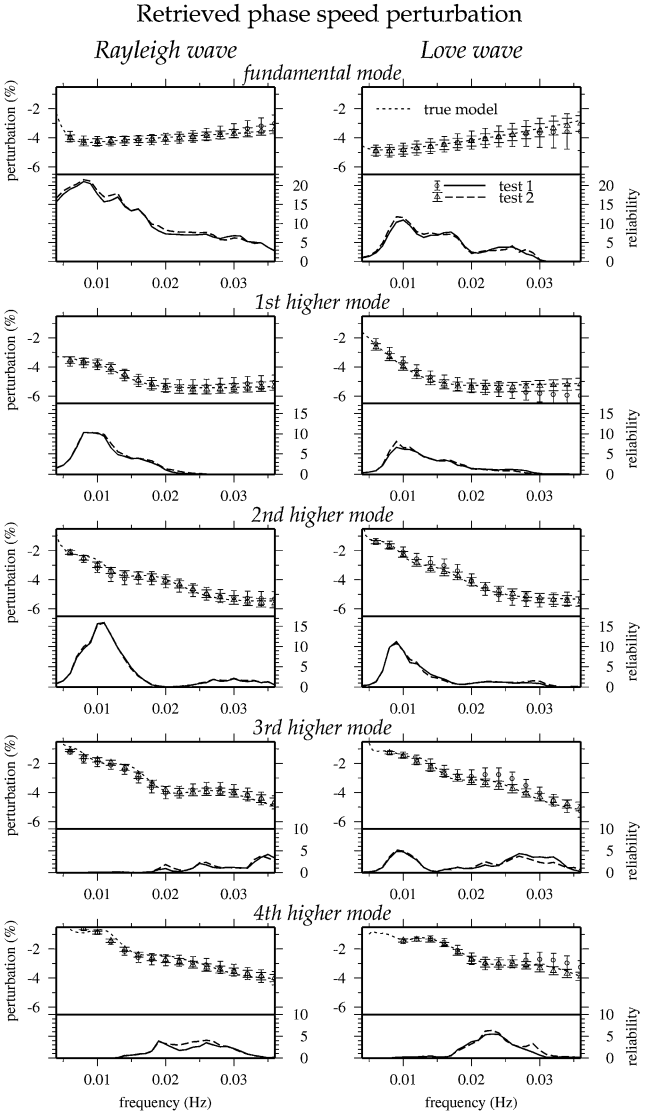

Figure 6. Phase speeds and the reliability parameters of the first five mode branches measured from the best-fitting 1-D models shown in Figs 5 and 8. Error bars are estimated from standard deviations of the best 1000 models.

are very close to the best-fitting models, so that this error estimation provides quite reasonable error bars around the estimated phase speeds. However, such rough estimates of errors are not quite sufficient for a quantitative evaluation of the measured phase speeds. Therefore, we introduce the reliability of the measurement as a way to evaluate our dispersion estimates.

3.2 Reliability of measured phase speed

One of the problems in dispersion measurement from a single seismogram is that it is not simple to evaluate meaningful errors or the reliability of the measurements. van Heijst & Woodhouse (1997) proposed a way to estimate the reliability by working with mode branch seismograms. Following their concept, we now redefine the reliability of the measured phase speeds that are recalculated from the 1-D models obtained through NA inversion.

First, let us introduce four types of seismograms: the observed seismogram $u^{\rm obs}(t)$; the full synthetic seismogram $u^{\rm syn}(t)$; the jth mode branch seismogram $u_j^{\rm syn}(t)$; and a residual seismogram for the jth mode, $\bar{u}_j^{\rm syn}(t)$ $(= u^{\rm syn}(t) - u_j^{\rm syn}(t))$. Then we further define the corresponding spectrograms; $S^{\rm obs}(\omega, t)$, $S^{\rm syn}(\omega, t)$, $S_j^{\rm syn}(\omega, t)$ and $\bar{S}_j^{\rm syn}(\omega, t)$ in the frequency–time (F-T) domain. The spectrograms in the F-T domain are obtained from a set of power spectra of the seismograms with moving time windows.

Before calculating power spectra, all seismograms are normalized with the maximum amplitude of the observed or the full synthetic seismograms. The power spectra are then estimated using the maximum-entropy method (MEM), which is well known to provide high-resolution spectral estimates even with short time windows (Lacoss 1971). The length of the time windows are chosen to be at least twice as long as the longest period of interest. Examples of the seismograms and their spectrograms are shown in Fig. 3. These are

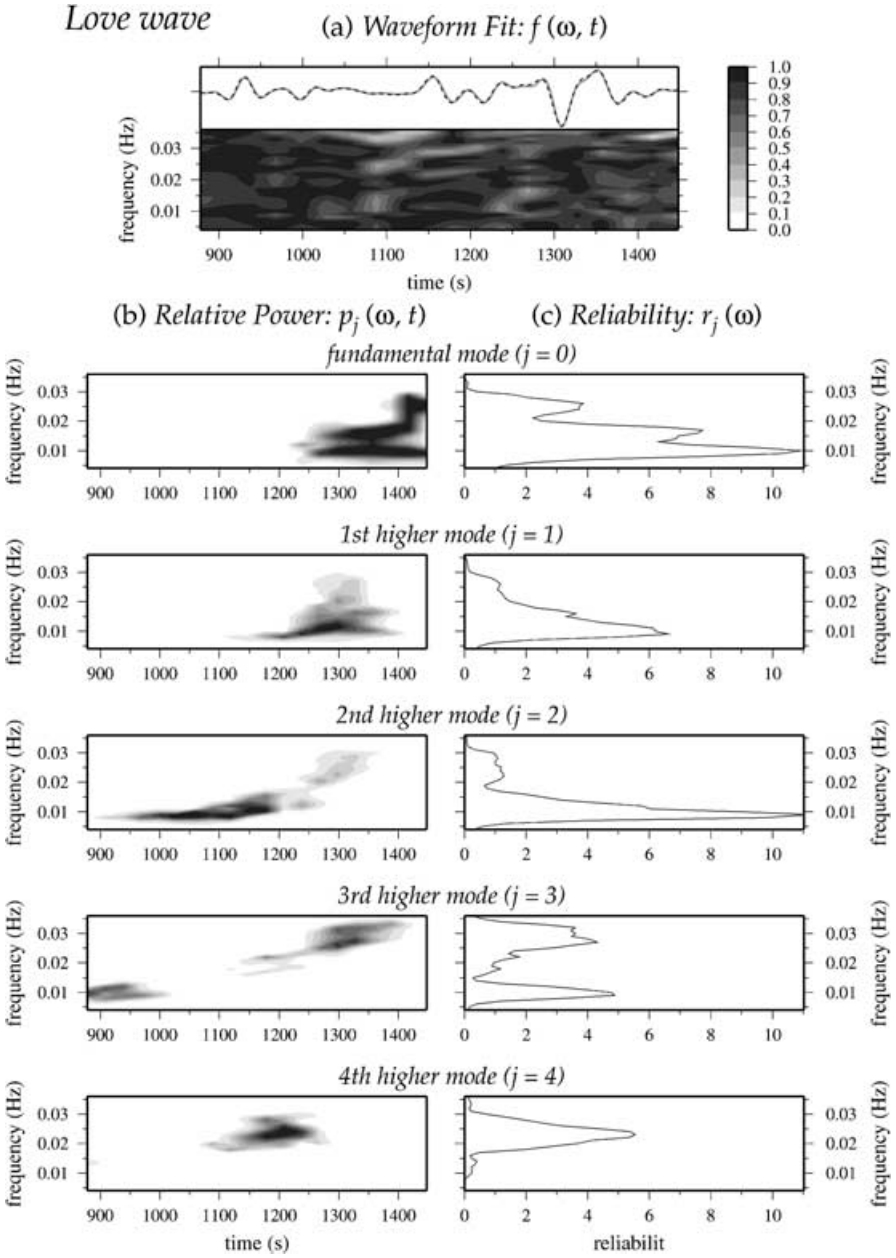

Figure 7. Same as in Fig. 4 but for the results of test I in Fig. 8.

calculated for the best-fitting waveforms obtained from a synthetic test described in Section 4. Such spectrograms in the F-T domain are used for defining a measure of waveform fit and the relative power of a mode branch in the following.

We quantify both the fit between synthetic and observed waveforms, $\mathbf{f}(\omega, t)$, and the relative power of jth mode, $\mathbf{p}_j(\omega, t)$, in a similar fashion to van Heijst & Woodhouse (1997), but we use spectrograms that can provide a direct estimate of the waveform fit and the relative power in the F-T domain. Both $\mathbf{f}$ and $\mathbf{p}_j$ are matrices. The components of the measure of waveform fit are defined as

$$f^{kl}(\omega, t) = f(\omega_k, t_l) = \exp\left[-\frac{|S^{\mathrm{obs}}(\omega, t) - S^{\mathrm{syn}}(\omega, t)|}{S^{\mathrm{syn}}(\omega, t)}\right], \qquad (7)$$

Table 1. Seismic events used for the data inversion with two cluster of events within $2^\circ \times 2^\circ$ regions in the Banda Sea and near Kermadec Island.

Event (Harvard Catalogue)	Lat.	Long.	Depth (km)	Scalar moment (dyne cm)
041991D	−6.93	129.51	113.0	1.88×10^{24}
101591D	−6.52	130.07	146.0	2.05×10^{24}
012093H	−7.24	128.60	33.0	4.91×10^{24}
100593B	−6.14	128.92	37.0	4.03×10^{24}
122595E	−6.94	129.18	150.0	4.70×10^{24}
111196A	−32.54	−179.05	33.0	1.67×10^{24}
100797B	−31.84	−178.32	33.0	6.69×10^{24}
122598B	−33.05	−179.32	78.2	2.90×10^{24}
091099F	−32.83	−178.27	33.0	6.37×10^{24}

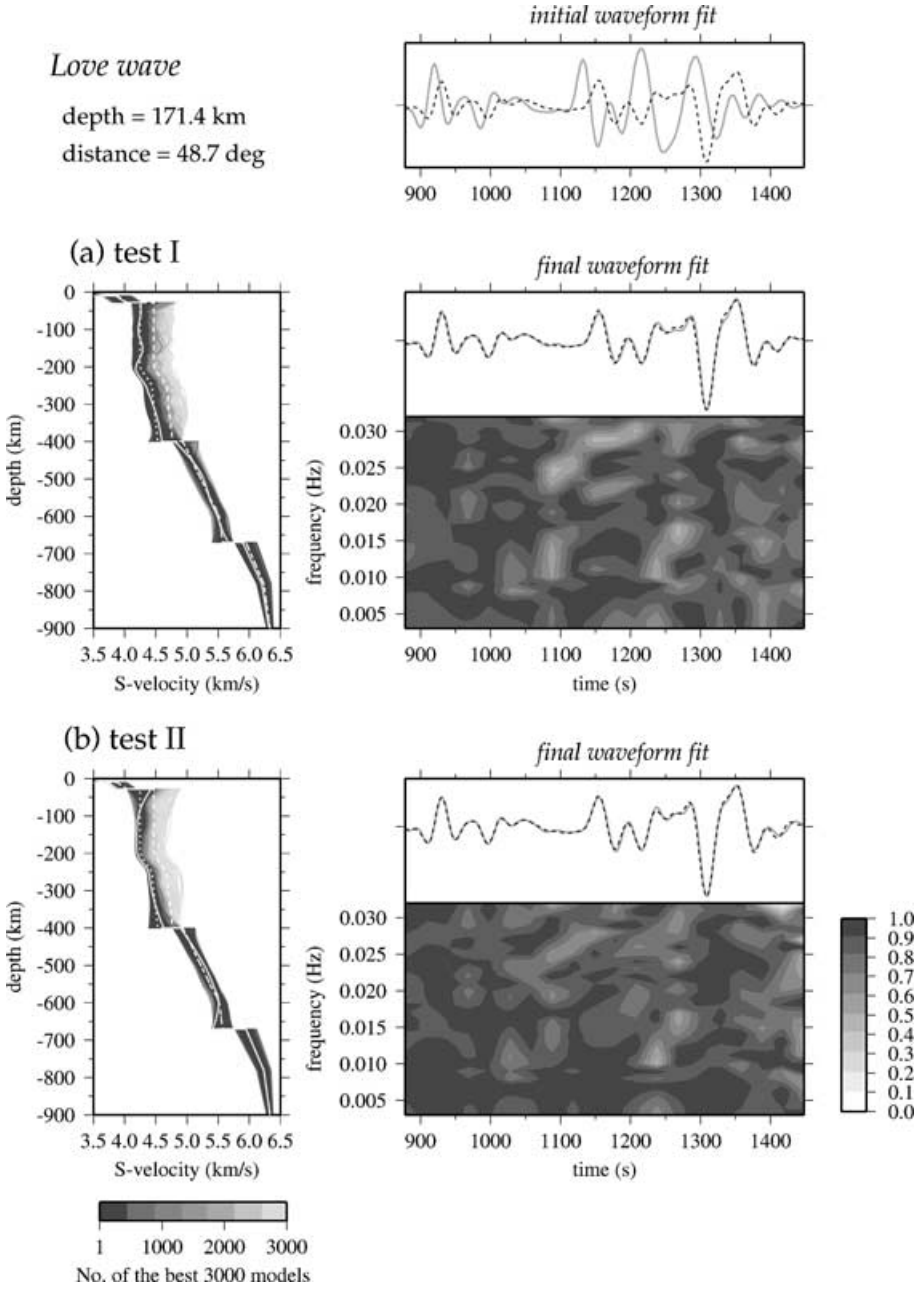

Figure 8. Same as in Fig. 5 but for a synthesized Love wave.

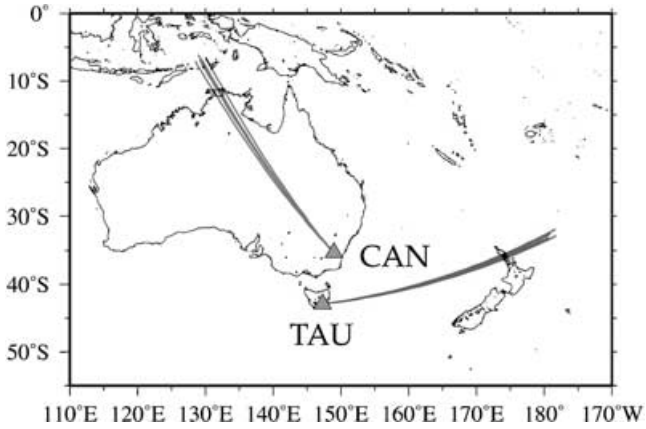

Figure 9. Ray paths for the source–receiver pairs used in the comparative inversions. Five events in the Banda Sea region and four in the Kermadec region are used, chosen from clusters within a $2^\circ \times 2^\circ$ zone.

where the indices k and l indicate the frequency and time component, respectively. f^{kl} becomes 1 when the amplitude of the spectrogram for observed and synthetic waveforms are identical, whilst it goes to 0 when the misfit between these two spectrograms becomes large.

The components of the measure of relative power of the jth mode, $\mathbf{p}_j$, are defined as:

$$p_j^{kl}(\omega, t) = p_j(\omega_k, t_l) = 1 - \exp\left[-W_j(\omega, t)\frac{\left|S^{\mathrm{syn}}(\omega, t) - \bar{S}_j^{\mathrm{syn}}(\omega, t)\right|}{\bar{S}_j^{\mathrm{syn}}(\omega, t)}\right], \quad (8)$$

where $W_j(\omega, t)$ is a weight function that works as an F-T domain filter to suppress the contribution from other modes, and is defined as the spectrogram of the jth mode branch seismogram normalized to its maximum value, $\max[S_j^{\mathrm{syn}}(\omega, t)]$,

$$W_j(\omega, t) = S_j^{\mathrm{syn}}(\omega, t) \Big/ \max\left[S_j^{\mathrm{syn}}(\omega, t)\right]. \quad (9)$$

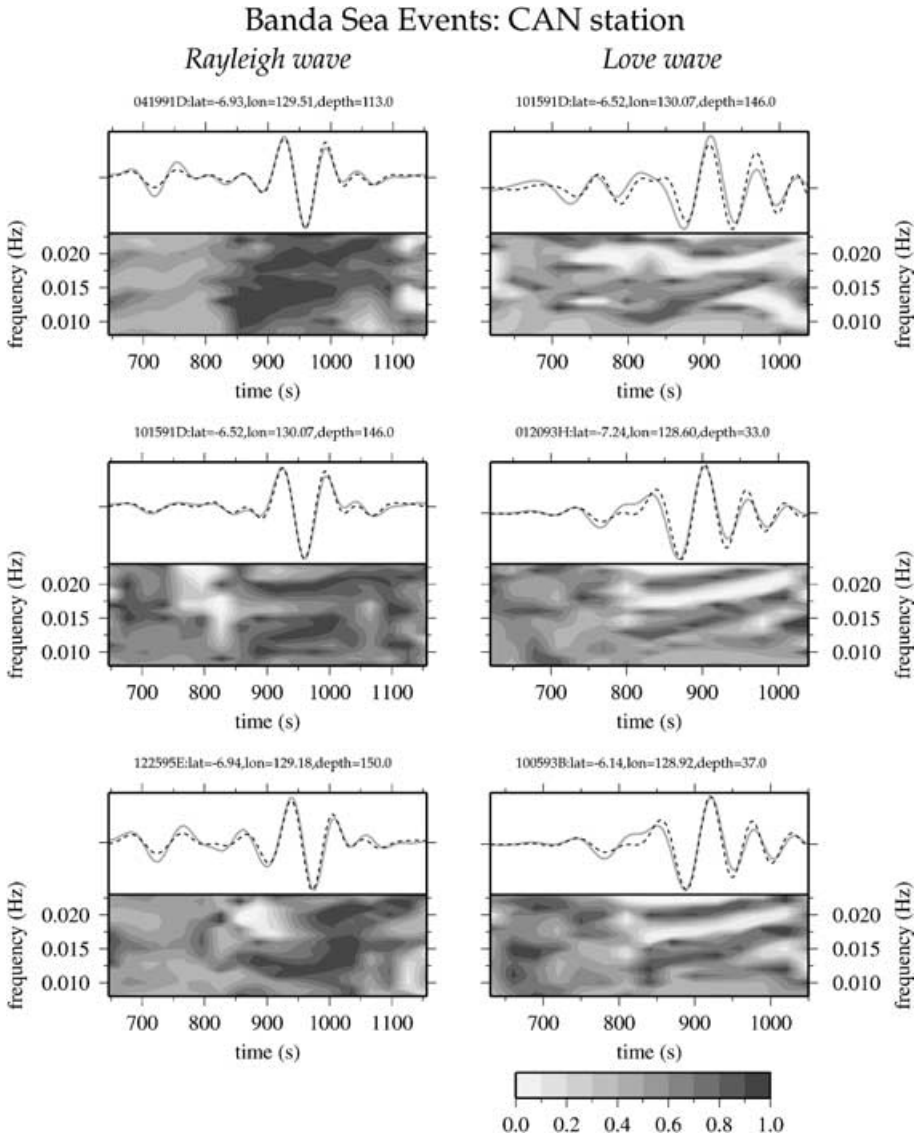

Figure 10. Final waveform fits and diagrams of the fit in the F-T domain for the paths from the Banda Sea region to the CAN station.

p_j^{kl} becomes 1 when the jth mode dominates the spectrogram and there is no contribution from the other modes, and becomes 0 if the jth component does not contribute to the spectrogram at all.

The reliability of the measurement can be calculated from the inner product of rows of the two matrices f^{kl} and p_j^{kl} at each frequency,

$$r_j(\omega) = n_t \sum_l p_j^{kl} f^{kl}, \tag{10}$$

where n_t is a normalization factor for the reliability parameter. Since the reliability is estimated by summing up the product of the relative power and the waveform fit within a finite time window, the estimated values depend on the length of the chosen window. In this study, we chose n_t so that the reliability becomes 1 when both p_j and f are 0.7 for 30 s. This criterion can be interpreted as being equivalent to a perfect relative power and waveform fit (both p_j and f are 1.0) for a 15 s time window. The maximum value of reliability depends on the length of the time span for which waveforms are matched and a particular mode branch is sufficiently energetic.

An illustration of the waveform fit $\mathbf{f}(\omega, t)$, relative power $\mathbf{p}_j(\omega, t)$ and reliability $r_j(\omega)$ is displayed in Fig. 4 for the results of the synthetic test shown in Fig. 5. In this example, the waveform is almost completely recovered and the relative power of the fundamental mode is almost 1 for 300 s in a time window around 0.01 Hz. This results in very high values (over 20) of the reliability parameter, because of the normalization of the reliability so that it is 1 when perfect recovery is achieved for just a 15 s time span.

4 SYNTHETIC TESTS

The non-linear inversion technique using NA has been applied to synthesized seismograms of both Rayleigh and Love waves. Synthetic tests have been performed with a uniformly perturbed 1-D model that contains −5 per cent shear wave speed perturbation from the PREMC model between Moho and 400 km. This perturbed model is used as a true model, whereas the PREMC model is used as a reference model for all the synthetic tests in this section. Two types of tests are carried out using different parametrizations.

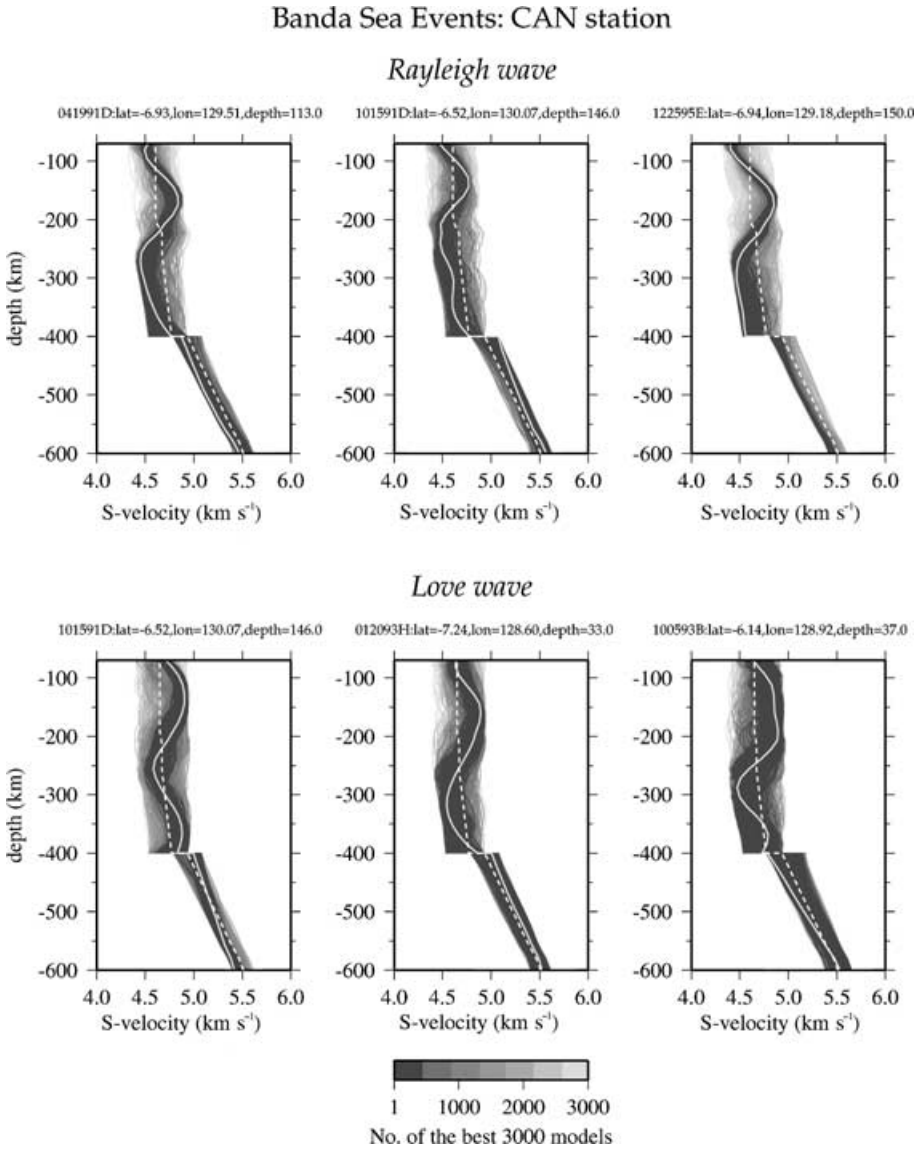

Figure 11. Density plots of 3000 1-D shear wave speed profiles obtained from NA inversion for the waveforms shown in Fig. 10. The best-fitting model is drawn in a solid white line and the reference model in a dashed line.

We used 16 B-splines ($M_1 = M_4 = 1$, $M_2 = 10$, $M_3 = 4$) for the first test (test I) and 12 B-splines ($M_2 = 6$ and the others are the same as test I) for the second test (test II). An event in the Vanuatu region with a depth of 171.4 km is used, and waveforms are calculated for a station NWAO in southwestern Australia for which the epicentral distance is 48.7°. The input seismograms for a true model (PREMC, −5 per cent) are calculated exactly. 3000 S-velocity models are generated by NA for each test and we measure phase speed perturbations obtained from the model with minimum misfit.

4.1 Rayleigh waves

The results of two synthetic tests for Rayleigh waves are shown in Figs 4 and 5. Diagrams of waveform fit and relative power for the Rayleigh-wave tests (Fig. 4) are calculated from the input seismogram and the best-fitting synthetic seismogram for test I. In the diagram of relative power for each mode branch, we can see that the fundamental mode is well separated from the higher modes. This fact results in a higher relative power for the fundamental mode that leads to higher reliability in the phase speed measurement. The first and second higher modes are also well separated from the other modes and they also have higher reliabilities.

The final waveform and the input observation match well and the overall features of the 1-D models are well retrieved for both test I and test II (Fig. 5). The best-fitting waveforms for these tests are almost identical, although the retrieved models show slight discrepancies.

In Fig. 6 (left-hand column), phase speeds as well as the reliability of the first five mode branches measured from the best-fitting 1-D model for both tests are shown. The errors of the phase speed measurements are estimated from the standard deviation of dispersion curves for the best 1000 models. The true perturbation of phase speed is almost completely recovered by the inversion, especially for the frequency ranges where the estimated reliability is high enough. If the reliability is low, for example below 0.013 Hz in the fourth-higher mode, we can see some differences between the true and the retrieved phase speeds. Although the retrieved path-specific 1-D models have differences in some depth ranges as seen in Fig. 5, the estimated phase speed perturbations for these models are almost identical, which can be expected from the very good correlation of the best-fitting waveforms.

4.2 Love waves

The same synthetic tests are also applied to the Love wave case. Diagrams of the relative power for several mode branches (Fig. 7) show that the higher-mode branches as well as the fundamental mode overlap over a wide time interval. This reduces the relative power of the fundamental and higher-mode Love waves, and results in lower reliabilities than for Rayleigh waves. This overlap of the fundamental and higher-mode Love waves also makes it difficult to analyse Love wave dispersion accurately.

The differences between the retrieved 1-D models for Love wave tests (Fig. 8) are much clearer than those for the Rayleigh wave, although both models with minimum misfit are quite close to the true model. The waveforms calculated for these models are still very similar and the shape of the input waveform is almost completely recovered.

Phase speeds measured from the best-fitting models are shown in the right-hand column of Fig. 6. As seen in the case of Rayleigh waves, the true phase speed perturbation is reconstructed very well for the frequency ranges with high reliabilities. Despite the significant differences between the 1-D models retrieved with different parametrizations, the estimated phase speeds are almost identical. This suggests that we can achieve stable multimode phase speed measurements for sufficiently energetic mode branches in a seismogram even with overlapping mode contributions. The tests also demonstrate that the reliability parameter will be a very useful indicator in evaluating measured phase speeds.

From the results of the synthetic tests, we may say that any 1-D model can be a good representation for multimode phase speeds as long as synthetic waveforms are well matched to observations. The results strongly support our assumption that path-specific 1-D models are a good representation of multimode phase dispersion rather than a direct representation of an actual Earth model. It is also important to note that, even though the path-specific 1-D models are not unique, this does *not* mean that the existing 3-D models based on such 1-D models are unreliable. We would be able to extract some robust information concerning the 3-D structure from an ensemble of 1-D models for a number of paths, even if each 1-D model has some degree of non-uniqueness.

5 APPLICATION TO OBSERVED SEISMOGRAMS

The non-linear inversion method is illustrated by application to two sets of surface wave paths in the Australian region so that we can assess the results of inversion by a comparison of similar paths. Seismic events over very small areas (within 2° × 2°) in the

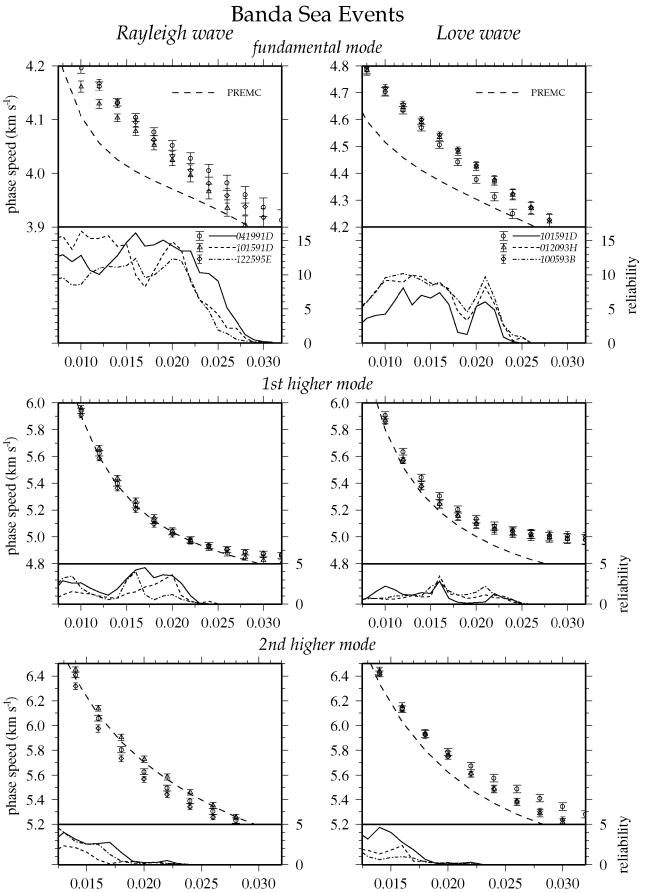

Figure 12. Phase speeds and the reliability parameters for the first three mode branches measured from the best-fitting 1-D profiles in Fig. 11. Error bars are estimated from standard deviations of the best 1000 models.

Banda Sea region in Indonesia and near Kermadec Island are chosen (Table 1). The NA inversions are performed for two sets of paths, from the Banda Sea to CAN station in southeastern Australia and from Kermadec to TAU station in Tasmania (Fig. 9).

We first check the radiation pattern from the source using Harvard Centroid Moment Tensor (CMT) solutions (e.g. Dziewonski *et al.* 1981), and seismograms that are near the nodal direction of Love or Rayleigh waves are discarded. Following the criteria of Lebedev (2000) for reducing uncertainties in the phase speed measurements using CMT solutions, the threshold values for the nodal direction have been determined so that the radiation amplitude is less than half of the maximum surface wave radiation. An appropriate reference model is constructed by perturbing the shear wave speed in the uppermost mantle for the PREM or PREMC model. The data adaptive procedure for finding an appropriate reference model is summarized in Appendix A. The instrument response is deconvolved from each of the waveforms. The NA waveform inversion is then applied to the observation using the reference model adapted to the data. The frequency bands for the multiple bandpass filters used in the data inversions are 8–12, 10–15, 12–18, 15–22 and 18–25 mHz. Over 3000 1-D shear velocity models are obtained from each path inversion and we select the model with minimum misfit for calculating multimode phase speeds of surface waves. The best 1000 models are used to estimate standard errors for the dispersion measurements.

5.1 Continental path: Banda Sea to CAN

The paths from the Banda Sea to the CAN station mainly pass through the Australian continent where we can expect fast wave speeds as revealed in recent tomography models for the Australian region (e.g. Simons *et al.* 1999; Debayle & Kennett 2000a). The results of the waveform fits and the corresponding fitting diagrams for the F-T domain are shown in Fig. 10. In most cases, the waveform fits are fairly good for fundamental-mode Rayleigh waves. The waveform match is also quite good for Love waves below 0.015 Hz, but becomes worse for higher frequencies around 0.02 Hz. Surface waves passing through thick continental crust tend to be contaminated by the effects of strong scattering, especially for higher frequencies and Love waves are more sensitive to such shallow

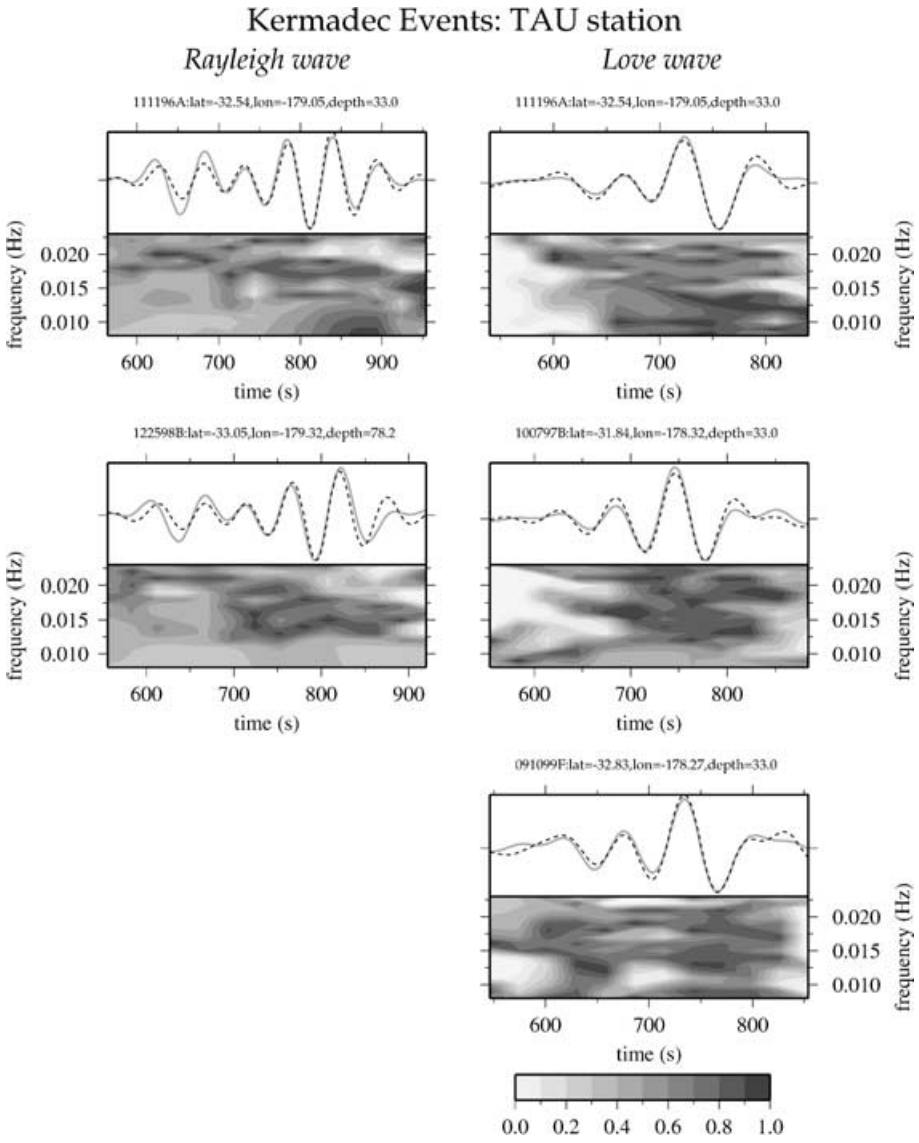

Figure 13. Same as in Fig. 10 but for the paths from the Kermadec region to the TAU station.

structures. Thus, the discrepancies at the higher frequencies can be ascribed to the effect of strong scattering caused by the thick continental crust of Australia that cannot readily be explained by ray theoretical synthetic waveforms.

Path-specific 1-D models for the paths from the Banda Sea to the CAN station are displayed in Fig. 11. A prominent feature of these models is that they all have high velocities in the depth range from 100 to 250 km. These high shear wave speeds are well correlated with a 3-D model of this region (Debayle & Kennett 2000a). The high wave speed zone in the 1-D models tends to be thicker for Love wave models, which is also consistent with the tomographic models for the region with larger *SH* wave speed anomalies than *SV* wave speeds (Debayle & Kennett 2000b). Although the overall features of the retrieved models are similar, there still remain some discrepancies amongst these 1-D models, especially in the deeper part of the mantle (below 300 km), which in general cannot be well resolved by surface waves because of the exponential tails of the surface wave eigenfunctions.

The estimated phase speeds for Rayleigh and Love waves are shown in Fig. 12. For the fundamental mode, the phase speeds of both Rayleigh and Love wave are considerably faster than those for the PREMC model over the frequency range with a high reliability measure, whereas the higher-mode Rayleigh waves do not show such a strong velocity perturbation from the PREMC results. The higher-mode surface waves are sensitive to variations over a wider range of depth in the 1-D models and do not just reflect local heterogeneities contained in the upper part of the mantle. As a result, the higher-mode phase speeds usually have smaller perturbation from the reference model than the fundamental mode. The higher-mode Love waves also shows smaller perturbation from the PREMC model for those frequency ranges with a high reliability measure.

5.2 Oceanic path: Kermadec to TAU

We also applied the NA inversion approach to oceanic paths from the Kermadec region to the TAU station in Tasmania, for which most regional and global tomography models suggest rather low shear wave speeds. The final synthetic waveforms are fairly well matched to the observations (Fig. 13). Unlike the continental paths, the waveform fits for higher-frequency Love waves are as good as for lower frequencies.

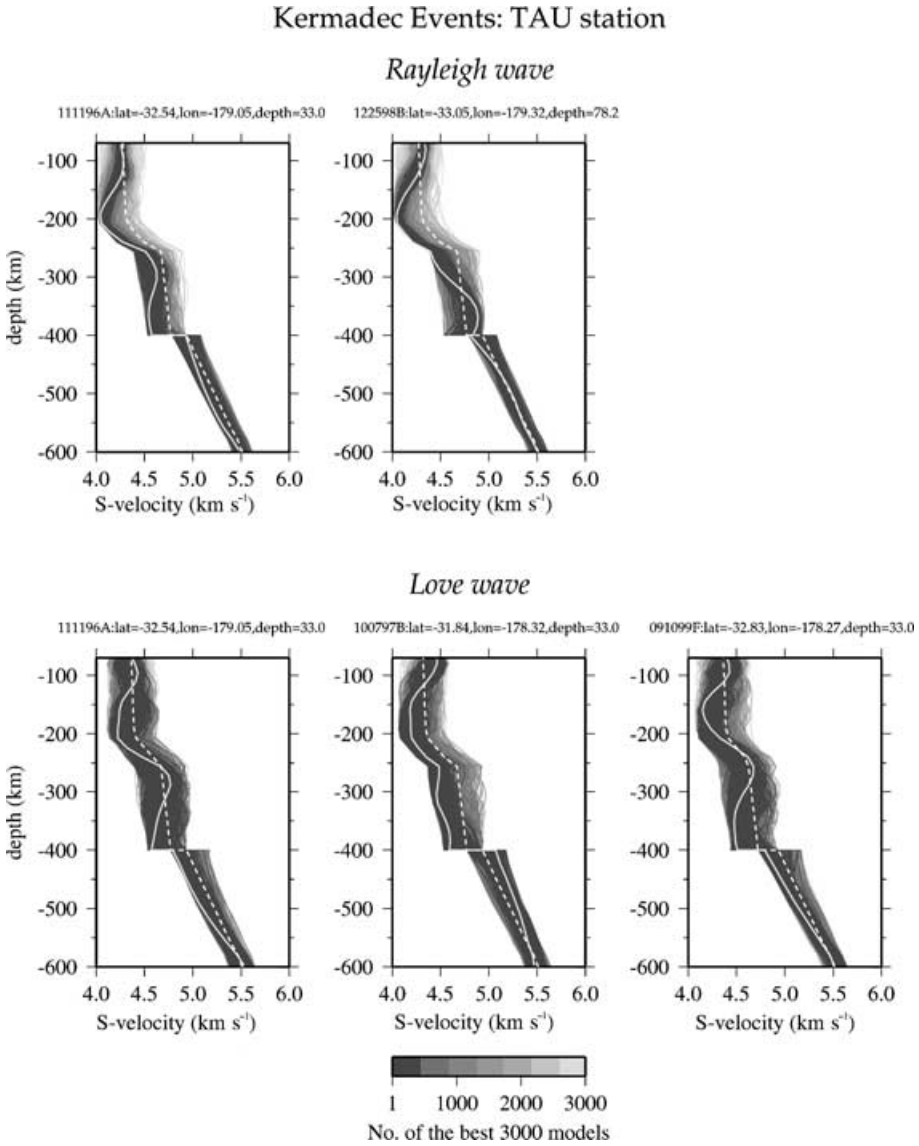

Figure 14. Same as in Fig. 11 but for the waveforms shown in Fig. 13.

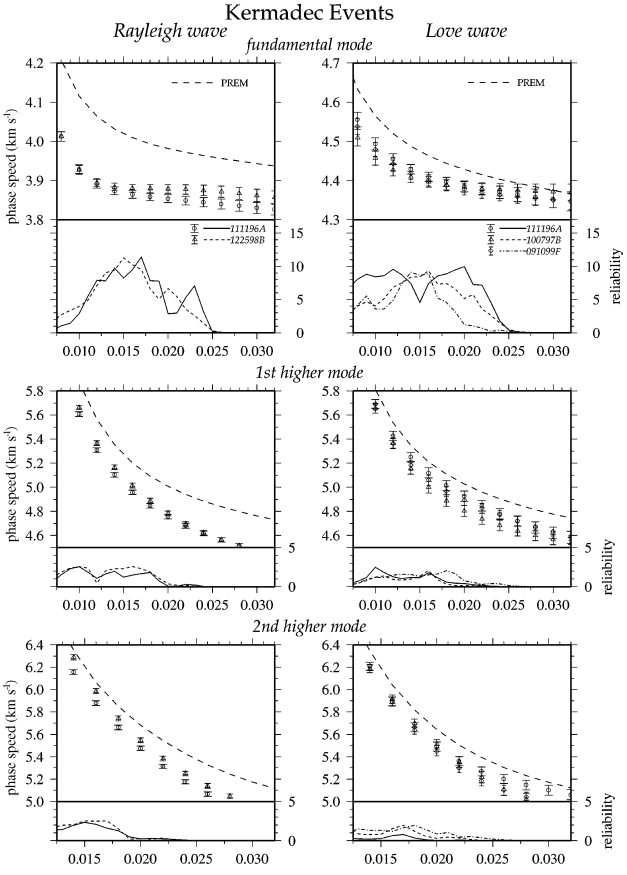

Figure 15. Same as in Fig. 12 but from the best-fitting 1-D profiles in Fig. 14.

The path-specific 1-D models in this region (Fig. 14) show a significant low shear wave speed zone between 100 and 200 km depth, and they are consistent with the existing 3-D model in this region (Debayle & Kennett 2000a). The deeper parts of these models, especially below 300 km, are rather contradictory. This is caused by the lack of sensitivity to the deep structure since the events used in this region are quite shallow (mainly a nominal 33 km) and do not excite enough energy in the higher modes, which are essential to reconstruct deeper structure. It should be emphasized that even though the 1-D models differ, the waveforms in Fig. 13 are fitted to a comparable level.

Phase speeds measured from the 1-D models (Fig. 15) for this region are consistently slower than the PREM model for both Rayleigh and Love waves. The perturbation of the phase speed from the PREM model is larger for the Rayleigh waves than for Love waves. This also implies a faster *SH* wave speed than the *SV* wave speed in this region, which is also seen in the polarization anisotropy model of Debayle & Kennett (2000b). The measured phase speeds from the different 1-D models agree well for the first few modes, for the frequency ranges with a high reliability measure. We therefore again see the effectiveness of deriving multimode dispersion measurements from the best-fitting 1-D profile of shear wave speed.

6 DISCUSSION

We have proposed the new technique to measure multimode dispersion from a single seismogram using non-linear waveform inversion with the neighbourhood algorithm. The NA technique itself is based on a simple concept and is quite effective in providing an intensive search of parameter space for models with smaller misfit. The waveform inversion based on this global search technique allows us to find models that fit the waveforms well and makes it possible to measure multimode phase speeds accurately. This style of inversion lets us treat both Love and Rayleigh waves independently using isotropic 1-D models. A data adaptive procedure has been developed to find an appropriate reference model for the perturbation analysis used in the synthetic seismogram calculations, as described in Appendix A. The concept of dispersion measurement from a path-specific 1-D profile is quite simple but the technique is found to be very powerful.

Even though the use of NA as a global search engine requires significantly more computation than linearized inversion methods, our technique has the capacity to analyse around 8000 seismograms within a month using a Compaq Alpha workstation with a 500 MHz processor. This may not be as fast as the mode stripping technique (van Heijst & Woodhouse 1997), but it is still efficient enough to analyse a large data set for regional scale studies. One of the advantages of the method that we have proposed in this paper is that surface waves with shorter epicentral distances can be used to measure multimode phase speed. This could not be achieved by any other single-station technique for phase speed measurement.

Synthetic tests clearly show that even if there is a substantial overlap of several mode contributions in a chosen time window, our fully non-linear approach can treat them in a proper manner. The reliability measures for the dispersion measurement can be a great help when we assess the retrieved phase speed, and can also be used as weighting factors for data in inversions for phase speed maps.

There still remain several aspects of the inversion that can be improved in the future. For example, allowing the Moho depth to change during the inversion will be crucial if we treat higher-frequency regional phases (more than 30 mHz), although working with such high-frequency ranges, which will require us to consider the effects of scattering or mode coupling, is beyond the scope of the current work. In this work, the amplitude term has been fixed and no variation in Q or eigenfunctions has been considered. Such an amplitude variation could also be incorporated in the current technique, with an increase in the number of parameters, which have to be considered in the NA inversion. In order to analyse a large data set with thousands of paths, it would also be desirable to automate the entire process of inversion. One of the possibilities for an automated procedure for waveform fitting is presented by Lebedev (2000) and his technique can also be applied with our inversion scheme.

The multimode phase speed measured using the new technique can be used to reconstruct phase speed maps for each frequency and for each mode. This would represent a linear inverse problem when we assume great-circle propagation. The phase speed distributions can be further improved in an iterative fashion by incorporating ray tracing for the different surface wave modes. Such an analysis is based on the phase speed measurement allows us to incorporate different types of information, such as polarization anomalies (Laske & Masters 1996; Yoshizawa *et al.* 1999) and finite-frequency effects of surface wave propagation (Yoshizawa & Kennett 2001). Phase speed maps obtained using such multiple information sources for the higher modes as well as the fundamental mode will lead us to more precise images of 3-D Earth models with enhanced vertical resolution.

ACKNOWLEDGMENTS

We wish to thank M. Sambridge for providing the NA programs and useful discussions. We are also grateful to B. Romanowicz and J. Trampert for their thoughtful and constructive reviews.

REFERENCES

Cara, M., 1978. Regional variations of higher Rayleigh-mode phase velocities: a spatial-filtering method, *Geophys. J. R. astr. Soc.,* **54,** 439–460.

Cara, M. & Lévêque, J.J., 1987. Waveform inversion using secondary observables, *Geophys. Res. Lett.,* **14,** 1046–1049.

Dahlen, F.A. & Tromp, J., 1998. *Theoretical Global Seismology,* Princeton University Press, Princeton, NJ.

Debayle, E. & Kennett, B.L.N., 2000a. The Australian continental upper mantle: structure and deformation inferred from surface waves, *J. geophys. Res.,* **105,** 25 243–25 450.

Debayle, E. & Kennett, B.L.N., 2000b. Anisotropy in the Australian upper mantle from Love and Rayleigh waveform inversion, *Earth planet. Sci. Lett.,* **184,** 339–351.

Dziewonski, A.M. & Anderson, D.L., 1981. Preliminary reference Earth model, *Phys. Earth planet. Inter.,* **25,** 297–356.

Dziewonski, A.M., Chou, T.-A. & Woodhouse, J.H., 1981. Determination of earthquake source parameters from waveform data for studies of global and regional seismicity, *J. geophys. Res.,* **86,** 2825–2852.

Ekström, G., Tromp, J. & Larson, E.W.F., 1997. Measurements and global models of surface wave propagation, *J. geophys. Res.,* **102,** 8137–8157.

Kennett, B.L.N. & Yoshizawa, K., 2001. A reappraisal of regional surface wave tomography, *Geophys. J. Int.,* in press.

Lacoss, R.T., 1971. Data adaptive spectral analysis methods, *Geophysics,* **36,** 661–675.

Laske, G. & Masters, G., 1996. Constraints on global phase velocity maps from long-period polarization data, *J. geophys. Res.,* **101,** 16 059–16 075.

Lebedev, S., 2000. The upper mantle beneath the western Pacific and southeast Asia, *PhD thesis,* Princeton University, Princeton, NJ.

Nakanishi, I. & Anderson, D.L., 1984. Measurements of mantle wave velocities and inversion for lateral heterogeneities and anisotropy, II. Analysis by the single-station method, *Geophys. J. R. astr. Soc.,* **78,** 573–617.

Nataf, H.C. & Ricard, T., 1996. 3SMAC: an, *a priori* tomographic model of the upper mantle based on geophysical modeling, *Phys. Earth planet. Inter.,* **95,** 101–122.

Nolet, G., 1975. Higher Rayleigh modes in western Europe, *Geophys. Res. Lett.,* **2,** 60–62.

Nolet, G., 1990. Partitioned waveform inversion and two-dimensional structure under the network of autonomously recording seismographs, *J. geophys. Res.,* **95,** 8499–8512.

Ritzwoller, M.H. & Levshin, A.L., 1998. Eurasian surface wave tomography: group velocitites, *J. geophys. Res.,* **103,** 4839–4878.

Sambridge, M., 1999a. Geophysical inversion with a neighbourhood algorithm I. Searching a parameter space, *Geophys. J. Int.,* **138,** 479–494.

Sambridge, M., 1999b. Geophysical inversion with a neighbourhood algorithm II. Appraising the ensemble, *Geophys. J. Int.,* **138,** 727–746.

Simons, F.J., Zielhuis, A. & van der Hilst, R.D., 1999. The deep structure of the Australian continent from surface wave tomography, *Lithos,* **48,** 17–43.

Stutzmann, E. & Montagner, J.-P., 1993. An inverse technique for retrieving higher mode phase velocity and mantle structure, *Geophys. J. Int.,* **113,** 669–683.

Takeuchi, H. & Saito, M., 1972. Seismic surface waves, in *Seismology: Surface Waves and Free Oscillations, Methods in Computational Physics,* Vol. 11, pp. 217–295, ed. Bolt, B.A., Academic Press, New York.

Trampert, J. & Woodhouse, J.H., 1995. Global phase velocity maps of Love and Rayleigh waves between 40 and 150 seconds, *Geophys. J. Int.,* **122,** 675–690.

van Heijst, H.J. & Woodhouse, J.H., 1997. Measuring surface-wave overtone phase velocities using a mode branch stripping technique, *Geophys. J. Int.,* **131,** 209–230.

van Heijst, H.J. & Woodhouse, J., 1999. Global high-resolution phase velocity distributions of overtone and fundamental-mode surface waves determined by mode branch stripping, *Geophys. J. Int.,* **137,** 601–620.

Woodhouse, J.H., 1974. Surface waves in a laterally varying layered structure, *Geophys. J. R. astr. Soc.,* **37,** 461–490.

Yoshizawa, K. & Kennett, B.L.N., 2001. Determination of the influence zone for surface wave paths, *Geophys. J. Int.,* in press.

Yoshizawa, K., Yomogida, K. & Tsuboi, S., 1999. Resolving power of surface wave polarization data for higher-order heterogeneities, *Geophys. J. Int.,* **138,** 205–220.

APPENDIX A: DATA ADAPTIVE CORRECTION FOR A REFERENCE MODEL

The choice of a reference model to initiate waveform inversion is one of the critical problems for 1-D path inversions, especially where the surface waves have passed through regions with strong local heterogeneities. The non-linear inversion with NA is able to retrieve up to ±5 per cent velocity differences quite well. However, the calculation of the ray theoretical seismogram based on perturbation theory does not allow too large a velocity perturbation. We therefore need to use a proper reference model that is not too far away from the best-fitting model.

In regional studies, the most significant velocity variations that affect intermediate- to long-period surface waves (50–130 s) are generally contained in the uppermost mantle above 200–250 km. The fundamental mode surface waves in such an intermediate period range can usually be fitted to the synthetics fairly well by perturbing the shear wave speed structure of the uppermost part of the mantle.

In order to obtain a reference model that is adaptive to the specific paths, we create several Earth models by perturbing the shear wave speed in the upper mantle above 250 km from a modified PREM or PREMC model. The choice of PREM or PREMC is based on the nature of the regions through which the path passes. Before perturbing the initial reference models, we correct the crustal structure using a 3SMAC model (Nataf & Ricard 1996). The P-wave speed, density and Q of the reference model are fixed, and no perturbation of these variables is considered. We then directly measure the phase speed of the fundamental mode surface waves using a single-station method (see, e.g., Nakanishi & Anderson 1984) by comparing the observations with a synthetic seismogram calculated for a perturbed reference model. We generate several perturbed reference models and calculate the average perturbation of the measured phase speed from the new reference model within certain frequency bands (7–20 mHz). The new model with the minimum average phase-speed perturbation are used as a new reference model for the NA inversion.

An example of the process of searching for a new reference model from the PREMC model is displayed in Fig. A1. In this example, we generate 10 trial reference models with shear wave speed perturbation from −5 to 5 per cent with a 1 per cent increment. The perturbation of fundamental-mode phase speed measured from a 3 per cent perturbed PREMC model has a minimum average perturbation of 0.29 per cent. Hence we use the 3 per cent faster shear wave speed model as a new reference model for the NA inversion and recalculate the normal modes and their eigenfunctions for this model.

The comparison of initial misfits for different reference models are shown in Fig. A1(c). The initial misfit for the PREMC model is quite large and major discrepancies are seen for the fundamental mode. However, the synthetic seismograms for the 3 per cent faster reference model matches well to the observed seismogram even before the NA inversion. This process may seem somewhat coarse, but we do not require rigorous calculations of the reference model at this stage, because finding a data adaptive reference model is just a preliminary process for the subsequent non-linear waveform inversion. The objective of the data adaptive procedure for estimating a reference model is to keep the required perturbations within ±2 per cent, for which the first-order perturbation theory should work well.

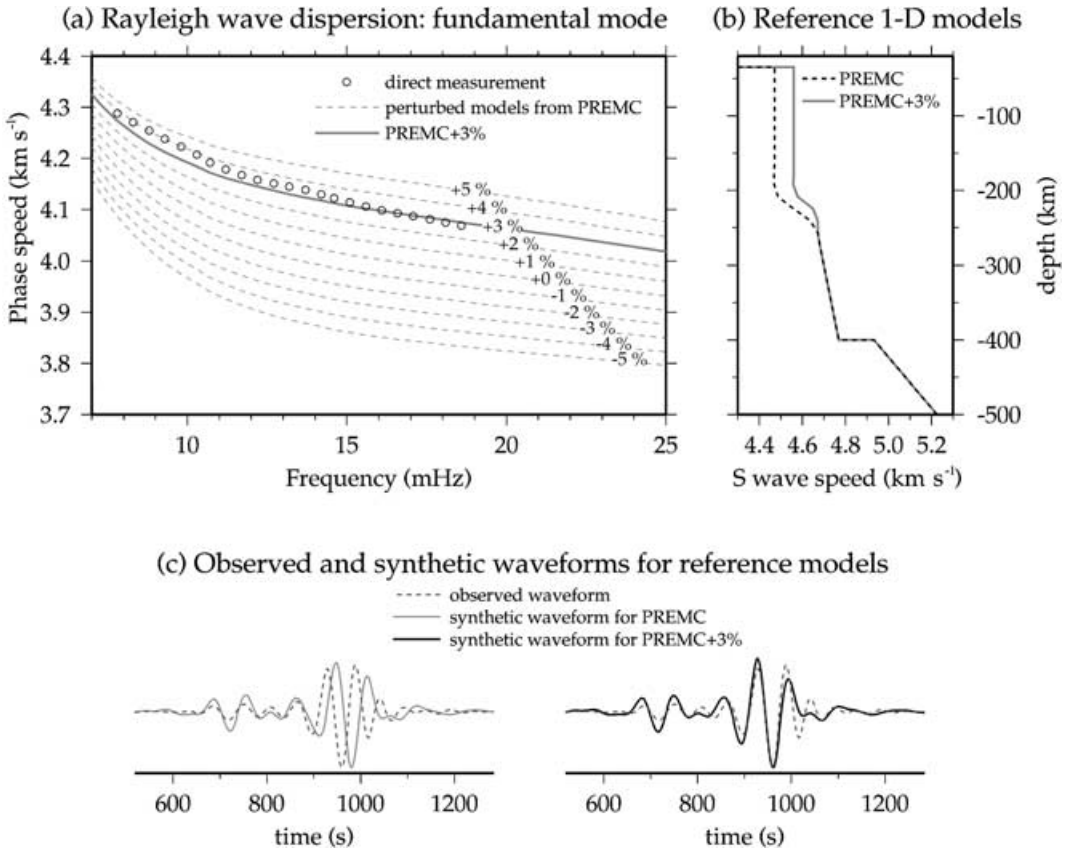

Figure A1. An example of the data adaptive search for the reference model. (a) Dispersion curves of the fundamental mode Rayleigh wave. The phase speed measured directly from the observations is plotted with circles and dispersion curves calculated from perturbed reference models are shown as grey dashed lines. (b) 1-D shear wave speed profile of the PREMC model and the new reference model with a 3 per cent faster wave speed in the upper 250 km. (c) Initial waveform fits for original and updated reference models.